Special Collection

Probing Individual Cuprous Oxide Microcrystals towards Carbon Dioxide Reduction by using In Situ Raman-coupled Scanning Electrochemical Microscopy

Matthias Steimecke,* Ana María Araújo-Cordero, Emil Dieterich, and Michael Bron*[a]

Dedicated to Wolfgang Schuhmann on the occasion of his 65th birthday.

In this work, the simultaneous investigation of a single cuprous oxide microcrystal towards CO_2 electroreduction (CRR, CO_2 reduction reaction) by using Raman microscopy and scanning electrochemical microscopy (SECM) is shown. Cu_2O microcrystals were electrochemically crystallized on an indium-doped tin oxide-substrate (ITO). Structural changes of the Cu_2O microcrystal are observed *in situ* by Raman microcopy, which indicates their fast conversion into elemental Cu at low overpotentials. Simultaneously, detection of products of the CO_2 reduction is carried out electrochemically using the sample-generation tip-collection mode (SG/TC) of SECM and formate ions are the main product of CRR, as detected by a 10 µm Pt ultramicroelectrode (UME). Thus, with our approach, the very beginning of the CRR (onset potential), potential-dependent product formation as well as structural changes in the catalyst can be precisely investigated.

Introduction

Global warming and its effects on nature and the environment caused by continued greenhouse gas emission is a widely accepted fact. Great efforts have to be made to counteract this dramatic development. In the future, it will not be sufficient to lower the emission of the major greenhouse gas, carbon dioxide, but it will be necessary to develop strategies of capture and storage to actively reduce the atmospheric CO_2 concentration. The electrochemical CO_2 reduction (CRR) is an approach which might use energy from renewable sources to convert this greenhouse gas into useful storable molecules. However, this approach requires stable electrode materials with low overpotential and high current densities. Besides a wide variety of materials, copper-based electrodes have turned out to be active towards the electrochemical CRR.[1] Cu and Cu_2O have been proposed as electrocatalysts in the CRR, producing single (methanol and formic acid) and multi-carbon molecules (ethanol, ethylene, and acetic acid).[2] Compared to the bulk material and deposited thin films, Cu_2O micro- and nanostructures improve the selectivity and performance in the CRR, allowing the investigation and comparison between their crystal facets, i.e., cubic with exposed (100) planes, octahedral with exposed (111) planes, and truncated octahedra with both planes exposed to the surface.[2,3] The syntheses of Cu, CuO, and Cu_2O micro- and nanocrystals with a controlled shape, size, and exposed crystal facets have been mainly reported by wet chemistry[3] or electrochemical methods.[4,5]

Various *in situ* techniques such as IR spectroscopy, X-ray absorption (XAS) and X-ray photoelectron spectroscopy (XPS) have been used to study materials during the CRR reaction as well as formed intermediates.[6] Recently, *in situ* surface-enhanced Raman spectroscopic was used to unravel the origin of selectivity in CRR on gold electrocatalysts.[7] In case of copper-based materials, Fu *et al.* reported a superficial electrochemical reduction of the Cu_2O nanoparticles to Cu during the CRR, as observed via *in situ* Raman spectroscopy, which could suggest that Cu has a strong influence in the reaction or even is the active catalyst.[3] Recently, *in situ* transmission electron microscopy in a liquid cell (LC-TEM) under CRR conditions showed restructuring of Cu_2O cubes and dendrite formation under reaction conditions.[8]

Additionally, scanning electrochemical microscopy (SECM) has been developed into a state-of-the-art *in situ* probing technique of electrocatalytic reactions.[9] The feedback mode of SECM has been used to detect reduction intermediates of the CRR in aqueous[10] and non-aqueous solution.[11] Furthermore, the sample-generation tip-collection mode (SG/TC) was used, either applying potentiodynamic modulation of the substrate and a constant potential at the microelectrode[12] or vice versa a constant potential at the substrate and potentiodynamic modulation at the microelectrode.[13] Regarding copper catalyst stability Filotas *et al.* studied corrosion effects and pH shift.[14]

By combining SECM with Raman microscopy, both electrochemical and spectroscopic information can be obtained with spatial resolution and as complementary datasets from the very same location of an electrode.[15,16] To allow for Raman probing

[a] Dr. M. Steimecke, A. M. Araújo-Cordero, E. Dieterich, Prof. Dr. M. Bron
Institut für Chemie, Technische Chemie I
Martin-Luther-Universität Halle-Wittenberg
Von-Danckelmann-Platz 4, 06120 Halle, Germany
E-mail: matthias.steimecke@chemie.uni-halle.de
michael.bron@chemie.uni-halle.de

Supporting information for this article is available on the WWW under https://doi.org/10.1002/celc.202101221

An invited contribution to the Wolfgang Schuhmann Festschrift

from the backside, a setup was suggested using transparent electrode materials, while the microelectrode of the SECM probes the sample from above.[15] In the present work, this approach was used to study CRR on cuprous oxide. Cu_2O individual microcrystals were electrochemically deposited onto a transparent ITO substrate. Simultaneous structural and electrochemical characterization was carried out as a proof of principle and to demonstrate that a detailed understanding of the *in situ* CRR catalytic reactions and its main products can be achieved with this approach.

Results and Discussion

Cuprous oxide is electrodeposited onto a transparent electrode material (ITO) from Cu^{II} solution by applying a constant potential. Reductive currents are observed during the whole deposition time. The respective chrono-amperometric curves are shown and discussed in Figure S1a and the text in the Supporting information. Morphological characterization of the deposited sample is summarized in Figure 1.

Figure 1a shows the X-ray diffractogram of a prepared sample and the corresponding Cu_2O pattern is comparable to those reported in literature[5,17] and the corresponding Miller indices are assigned. Additionally, two peaks of elemental Cu were identified.[18] The positions of the peaks corresponding to the ITO substrate were obtained from a diffractogram of the bare ITO conductive glass and marked with a red asterisk (*) in the figure. The obtained XRD is consistent with the reported results without any significant intensity differences of the Cu_2O. The unexpected Cu peaks possibly stem from slight changes in the local electrodeposition potential by a different reference electrode or the relatively large substrate. The diffractogram suggests a slightly preferred (111) crystallographic orientation of the deposited Cu_2O microstructures, due to its higher intensity than the other X-ray patterns. In order to further confirm the presence of Cu_2O in the sample Raman spectra were recorded at the microcrystals (Figure 1b). Prominent peaks are found at 218, 523 and 610 and 650 cm^{-1} which can be assigned to Cu_2O. Here, only the peak at 523 cm^{-1} is a "real" active Raman mode of the Cu_2O lattice vibration of the threefold-degenerate T_{2g} symmetry. All others peaks are silent (forbidden) or IR-active modes which are all appearing independently from the synthesis route and are possibly present due to copper split vacancy and point defects in p-type Cu_2O.[19] Homogeneity of the microcrystals was analyzed by Raman mapping experiments and the intensity of most prominent peak at 218 cm^{-1} was visualized in the color-coded image (Figure 1c). The Raman mapping was performed in a confocal mode with constant height above the sample and depending on the orientation of the crystals some planes can be parallel to (the crystal in the lower part of the image) and some run out of the laser focus (both crystals in the upper part of the image) resulting in decreased signal intensity. In this way, the different orientations of the crystals with planes, edges and corners appear and a 3D structure becomes visible. These structural features were additionally confirmed by scanning electron microscopy (SEM). Defined cubic shapes of the Cu_2O microstructures with planes (100) exposed to the surface can be seen from Figure 1d. The obtained microstructures correspond to those reported by McShane et al.[5] Their exposed surface area was calculated, determining the length of the crystals to calculate the area of a plane and multiplying by the five faces of each crystal. The main surface area of the individual microstructures is 31.5 μm^2 with 6.7 μm^2 of standard deviation. Additionally, it was calculated that the Cu_2O microstructures occupied the 9.25% of the ITO surface when just the determined area in contact (one face) of the crystals is divided by the total area of the substrate (see Figure S2 in the Supporting information).

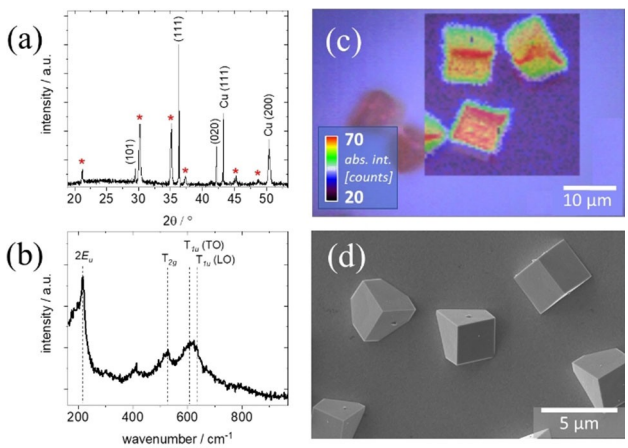

Figure 1. X-ray diffraction pattern (a), Raman spectrum (b) an optical image with a Raman mapping overlay using the most intense peak at 218 cm^{-1} (c), and a SEM image (d) of the grown of Cu_2O microcrystals on ITO. The asterisk in (a) mark the patterns of the ITO layer of the transparent, conductive electrode.

Electrochemical Characterization

Cyclic voltammograms of the prepared Cu_2O/ITO electrode were recorded in in CO_2-saturated 0.1 M $KHCO_3$. The results are shown in Figure S1b in the Supporting information. However, the information from such a CV is limited and only one pronounced reduction wave is observed at $E < -0.8$ V vs. Ag|AgCl|$KCl_{sat.}$ which is a result of carbon dioxide, bicarbonate reduction and/or hydrogen evolution. The limited information obtained by half-cell characterization techniques requires other experimental approaches to gain more detailed electrochemical information. Thus, the CRR at Cu_2O cubes was investigated with an *in situ* Raman spectrometer combined with a scanning electrochemical microscope.

In situ Raman-SECM Characterization

A schematic representation of the experimental setup can be found in Figure 2a and more details are presented in the literature.[15] The Cu_2O/ITO electrode is placed in a cell and the

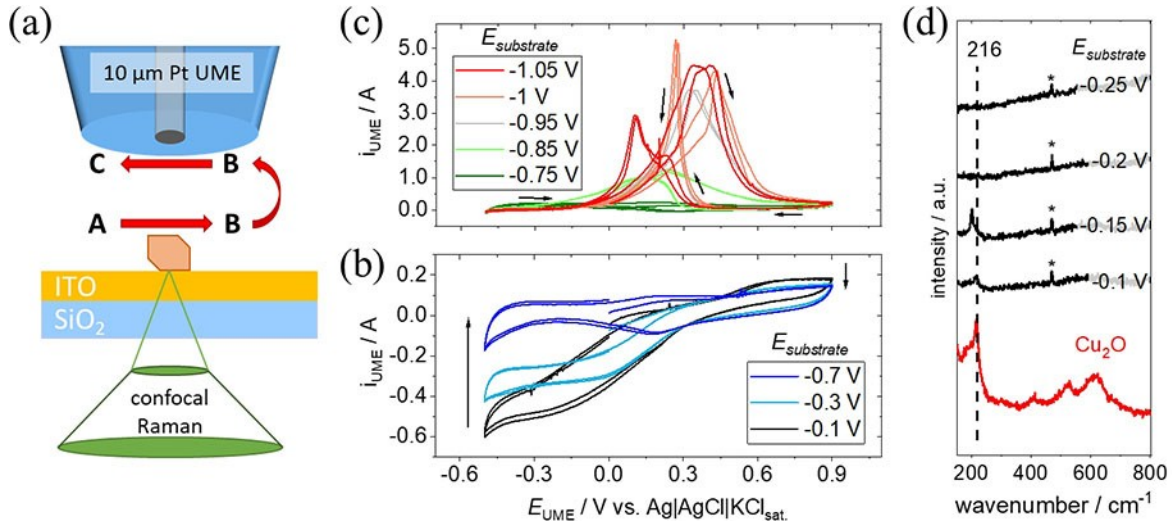

Figure 2. Experimental setup of the Raman-coupled scanning electrochemical microscope (a), selected cyclic voltammograms of the 10 µm Pt ultramicroelectrode in approximately 10 µm tip-to-sample distance to the Cu_2O microcrystal at various substrate potentials ($E_{substrate}$ from −0.1 to −1.05 V) (b, c); the arrows in (b) indicate the decrease of currents with decreasing substrate potential, whereas in (c) the curve progression is indicated for −1 V, as well as selected corresponding *in situ* Raman spectra, the asterisk indicates a peak from the quartz substrate (d).

probing by a microelectrode is realized from the topside while at the same time spectroscopic information is recorded from the bottom through the ITO substrate.

In the following, all potentials are referred to the Ag | AgCl | $KCl_{sat.}$ reference electrode. During the characterization procedure, the sample ("substrate") was progressively polarized from −0.1 V to −1.05 V ($E_{substrate}$) applying 50 mV steps. After each potential steps three consecutive CVs were recorded at the ultramicroelectrode (UME) in close proximity (~10 µm) to the Cu_2O microcrystal to detect molecules formed at the substrate electrode. Additionally, a Raman spectrum was recorded.

Beginning at $E_{substrate} = -0.1$ V (Figure 2b) the CV at the UME is dominated by reductive currents at $E_{UME} < 0.2$ V which are attributed to the reduction of oxygen present in the solution.[20] This is an expected result of a restricted saturation time with CO_2. Under the applied conditions, the limited stability of Cu_2O requires a fast *in situ* characterization after assembling the cell and inserting the electrolyte. Cell assembly and start of the experiment were carried out sufficiently fast and oxygen reduction, but no copper features, which would indicate Cu_2O structure dissolution, are present in the very first potential step CV. Beside restricted saturation time with CO_2, the cell is not closed to ambient air (due to the UME positioning system) which leads to additional oxygen contribution.

At the same substrate potential, oxidative currents can be observed at $E_{UME} > 0.5$ V which are caused by hydrogen peroxide oxidation.[21] This result indicates that Cu_2O already reduces oxygen at −0.1 V and an indirect pathway (2 + 2 electrons) of the oxygen reduction reaction (ORR) is taking place, leading to hydrogen peroxide as the product of the two-electron reduction. This was also confirmed by Zhang et al. studying copper close to the corrosion potential by SECM at a comparable pH value.[21] When lowering $E_{substrate}$ to −0.5 V both contributions to the UME current (ORR and hydrogen peroxide oxidation) decrease indicating the total conversion of oxygen in a four-electron reduction by the microcrystal structure. The corresponding Raman spectra (Figure 2d) of this potential region show the presence of Cu_2O which can be concluded from the peak at 216 cm^{-1} at −0.1 V. This peak shifts to lower wavenumbers ~200 cm^{-1} and vanishes at $E_{substrate} = -0.2$ V indicating the reduction of Cu_2O crystal to Cu at this potential.[22] This is also supported by an increased Raman signal baseline at $E_{substrate} < -0.2$ V resulting from the high reflectivity of Cu.

Starting from $E_{substrate} < -0.7$ V (Figure 2c) different oxidative current contributions can be observed at the UME which indicate product formation at the substrate and become more and more pronounced with more negative potential. The very beginning of a product evolution from the Cu_2O microcrystal can be found at −0.75 V. This is in accordance with the observation of a strong reductive current appearing at the substrate (Figure 3a). On closer examination of the consecutive CVs at −0.75 V and −0.8 V (Figure 2c), oxidative contributions can be observed in a broad potential region (between 0 and −0.5 V) at the UME which are attributed to oxidation of products evolved from the microcrystal. This potential can be considered as the onset potential (E_{onset}) of the CRR over the microcrystal. At $E_{substrate} < -0.8$ V two distinct peaks appear in the CV, in the forward (sweep to higher potentials) and backward scan, respectively. Both peaks increase when $E_{substrate}$ is lowered and a current maximum at the UME (~5 nA) is observed at $E_{substrate} = -1.0$ V. Afterwards, the current maximum of the backward CV scan decreases and its position shifts to lower potentials.

In the following, individual results of the *in situ* UME CVs will be discussed and current contributions will be assigned. For this purpose, it was necessary to evaluate current contributions of individual molecules under conditions equal to those of the

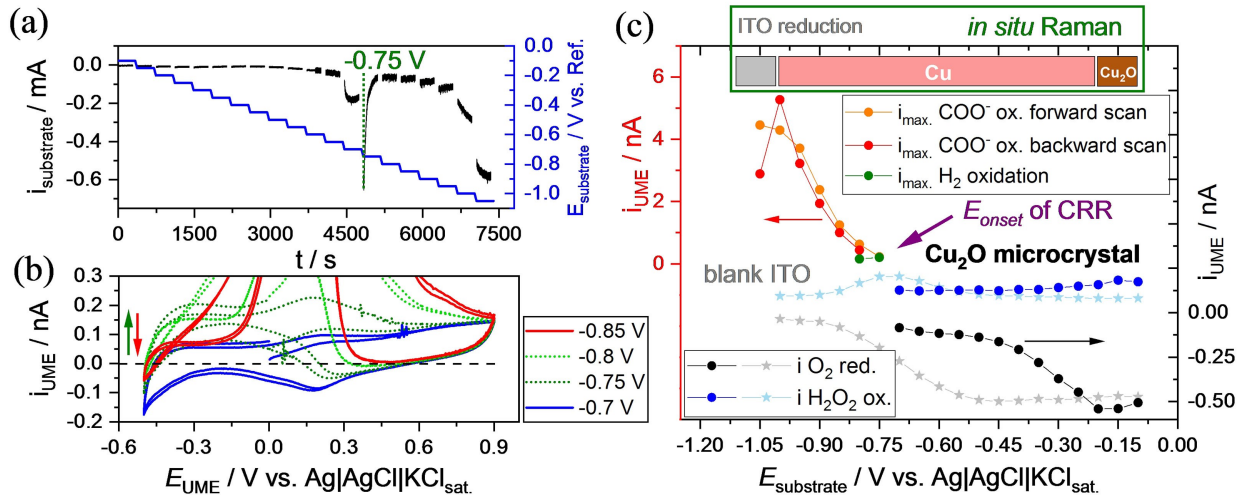

Figure 3. Current (black) and potential (blue) of the Cu_2O/ITO sample plotted over the *in situ* experiment time, in the gaps between the current steps Raman acquisition took place (a), corresponding CVs of the UME at selected potentials of the onset potential region where the arrow indicates the shift of Pt–H_{upd} region into positive current (due to hydrogen oxidation) and back (b) and a comprehensive evaluation of all datasets (c).

CRR experiments. Six relevant products of the CO_2 reduction reaction were individually added to a CO_2-saturated 0.1 M $KHCO_3$ solution, namely hydrogen, carbon monoxide, potassium formate, methane, methanol and ethanol, and CVs at an UME were recorded in the very same manner as in the *in situ* setup. All results and discussion about the reference molecule characterization can be found in Figure S3 and in the text of the Supporting information.

On the basis of this information the microelectrode response of the onset potential region is examined in more detail (Figure 3b). Here, the current contributions in the low-potential region of the UME CV (ca. −0.3 V) at −0.75 V substrate potential (Figure 3b) can be assigned to the oxidation of dissolved hydrogen that is formed in the very beginning of the CCR. At −0.8 V the contribution of hydrogen oxidation has already decreased and formate is additionally produced which forms the characteristic oxidation peaks in the forward and backward scans. Formate ions have already been reported as a main product and were used for SECM feedback experiments over Cu structures.[10] At −0.85 substrate potential no contributions of hydrogen oxidation can be found anymore in the and the Pt–H_{upd} region of the UME resembles that of the UME CV at −0.7 V $E_{substrate}$. Only formate ions can be detected at the UME during the following potential steps. It should be stressed here that the CVs in a potential region from −0.1 to −0.95 V are highly reproducible and the progression of the curves is nearly identical for each of the three consecutive CVs, so steady-state conditions during the *in situ* probing in this potential window can be assumed.

At potentials < −0.95 V the progressions of the consecutive CVs begin to differ (Figure 2c). Additionally, at −1.1 V a broad peak between 300–700 cm^{-1} is observed in the Raman spectra (not shown). Since copper is already fully reduced to its elemental state, a change of the substrate electrode has to be assumed. Under these conditions, it is known that the ITO substrate is irreversibly destroyed.[23] On the one hand, this finding is confirmed by strong reductive current increase at the substrate (Figure 3a) and on the other, it is also supported by an observable transparency loss and an increased opaqueness of the whole sample in the inverted microscope at this potential.[24] Additionally, pH shift caused by the ongoing CO_2 reduction may increase the local pH[25] in the gap between substrate and microelectrode which may explain the shift of the peak maximum of formate oxidation between −1 and −1.05 V.

Summarizing the information above, a general overview about the performed *in situ* experiment can be drawn (Figure 3c). In the upper part of this figure, the structural development of the sample and the substrate is visualized. The section in the middle summaries the formate oxidation currents obtained the UME CVs (see Figure 2c) as well as hydrogen oxidation, while in the lower part, the oxygen reduction respectively hydrogen peroxide oxidation currents (Figure 2b) are summarized. To further support the results, the procedure was also applied to a bare ITO substrate and the main results are also displayed in Figure 3c. The procedure was performed identically as for the Cu_2O/ITO sample, so, again small moieties of oxygen are present in the solution when the experiment started. However, in contrast to the Cu_2O/ITO sample, beginning oxygen reduction reaction was observed at far higher overpotential (−0.55 V) which was again accompanied by hydrogen peroxide formation as well. At lower potentials, none of the studied CO_2 reduction products could be detected electrochemically. This supports the use of the ITO substrate as transparent electrode material for the characterization of materials for the CRR in a potential window from 0 to −1.0 V.

Conclusions

Cuprous oxide microcrystals were homogeneously electrodeposited onto a transparent ITO electrode. The sample was morphologically and structurally characterized and afterwards

successfully investigated with an *in situ* Raman-SECM setup which allows a micrometer-precise probing of a single crystal.

The carbon dioxide reduction reaction (CRR) was probed by cyclic voltammetry at a platinum microelectrode and structural changes of the Cu_2O/ITO sample by Raman microscopy during reductive potential steps from −0.1 to −1.05 V. The microelectrode response suggests the formation of hydrogen at lower overpotentials and formate ions at higher ones, as confirmed by reference measurements, where these molecules were added on purpose. The onset potential of the CRR can be determined to be at −0.75 V which is in line with the occurrence of a strong reductive current increase at the substrate. Spectroscopic data suggests the early conversion of cuprous oxide to copper at −0.2 V.

For the chosen potential region ITO is a very useful substrate material and no relevant contributions to the CRR could be found, however, its application as transparent electrode material for optical probing is limited to values above −1 V under these conditions.

Experimental Section

Sample Synthesis and Ex Situ Characterization

In this study, Cu_2O microstructures were electrochemically synthesized using Indium-doped tin oxide (ITO) on quartz glass as electrodes, which are commercially available (PGO GmbH, Iserlohn). This substrate is used due to its optically transparent and conductive properties (~20 $\Omega\,cm^{-1}$), allowing the Raman characterization from the backside through the quartz substrate.

Beforehand, all samples were cleaned by immersion in 5 mL acetone, followed by 5 mL isopropanol in an ultrasonic bath for 5 minutes in each solvent. Initially, cuprous oxide (Cu_2O) microcrystals were electrochemically synthesized on the conductive surface of the ITO substrates following the procedure reported by McShane.[5] A three-electrode setup was used with cleaned ITO substrates as the working electrodes, a platinum wire as the counter electrode, and a saturated Ag|AgCl|$KCl_{sat.}$ as the reference electrode. All the experiments were conducted applying a constant potential of −0.02 V vs. the reference electrode for 300 s, in a 0.02 M $Cu(NO_3)_2$ aqueous solution at 60 °C prepared using Copper (II)-nitrate trihydrate (99–104 %, Lot: G3310, Fluka). The equipment used was a PGSTAT 302N Autolab potentiostat with Nova 2.1 software suite.

Once the electrochemical deposition was performed, the samples were rinsed abundantly with distilled water to remove the remaining ions. After synthesis, the Cu_2O microstructures were characterized by SEM, XRD, and Raman spectroscopy without a significant sample preparation before characterization and avoiding their destruction during the analysis. SEM images of the Cu_2O microstructures were taken by an FEI Versa 3D dual beam system microscope using a 5 kV acceleration voltage, 27 pA incoming beam current, 10.6 mm working distance, and ICE detector as operating conditions. X-ray diffraction pattern were recorded with a Bruker D8 Advance Bragg-Brentano X-ray Powder Diffractometer using Cu Kα radiation as source. Recordings were taken from 5° to 55° 2θ with step size of 0.01144 and 1 s integration time per step. Raman spectroscopy was performed using an InVia spectrometer (Renishaw) which was connected to both a microscope and an inverted microscope (both Leica). A tunable podule allows to change the beam paths for the respective microscope. A 532 nm laser (Renishaw, 500 mW) was used as excitation source. Both microscopes were equipped with different objectives (x50 and x100) which focus the laser on the sample and collect the scattered light (confocal). The scattered light was forwarded to a turnable grating (1800 l mm^{-1}) and further to a CCD camera. Spectra were recorded from 100–1000 cm^{-1}. In all experiments the spectrometer was adjusted to a peak at 520.4 cm^{-1} of a polycrystalline Si waver before. For mapping experiments, the sample was placed on a movable stage (Prior) providing 100 nm position resolution.

In Situ Raman-Coupled SECM Setup and Procedure

A details description of the combined *in situ* setup can be found elsewhere.[15] Briefly, a scanning electrochemical microscope (Sensolytics, Bochum) was added on top of an inverted microscope (Leica, Wetzlar) which is connected to the Raman spectrometer as described before. An electrochemical cell with the sample is mounted on a x-y stage for position control. Raman probing was realized from the bottom side of the cell whereas the ultramicroelectrode (10 μm (diameter) platinum wire in glass, RG = 30, Sensolytics, Bochum) was introduced from the top side into the cell which was filled with 0.1 M $KHCO_3$ (99 %, Carl Roth). The solution was continuously saturated by bubbling CO_2 gas (99.995 %, Air Liquide) and a pH = 6.8 can be assumed. Additionally, the cell was equipped with a counter (Pt wire, Goodfellow) and a Ag|AgCl|$KCl_{sat.}$ reference electrode (Meinsberger Elektroden). Including the UME and substrate all electrodes were connected to a bipotentiostat (PGSTAT128N, Metrohm) where the substrate with the sample serves a second working electrode. The positioning of the UME was realized by lowering it down until a blank region of the ITO substrate was touched. Afterwards the UME was lifted 10 μm and positioned above a single Cu_2O crystal. The whole procedure was optically controlled by the inverted microscope. Finally, the laser spot was focused on the middle of the microcrystal. Before the experiment the microelectrode was polished using 1.0 μm and 0.3 μm alumina polishing paper (Sensolytics, Bochum).

In the following procedure, the sample was polarized stepwise (50 mV $step^{-1}$) from −0.1 V to −1.05 V and the current was recorded. In parallel, three cyclic voltammograms between −0.5 and 0.9 V (scan rate 20 mV s^{-1}, start/stop potential 0 V) were recorded at the UME. Afterwards, the Raman acquisition was performed while the potential of the substrate was still applied. After the measurement had finished the next potential step was applied. For the sake of comparison, this procedure was repeated with a blank ITO substrate. All potentials are referred to the Ag|AgCl|$KCl_{sat.}$ reference electrode.

For the characterization of the reference molecules, mixtures of 0.1 M of the respective molecule, i.e. methanol (Rotisolv > 99,98 %, Ultra LC-MS, Roth GmbH), ethanol (absolute, 99.9 %, HPLC, Th. Geyer GmbH) and potassium formate (ReagentPlus, 99 %, Roth GmbH), in 0.1 M $KHCO_3$ were prepared and the solution was used in a half cell setup with continuous CO_2 saturation. Gaseous molecules, i.e. methane (2.5, Air Liquide), hydrogen (99.999 %, Air Liqiude) and carbon monoxide (10 Vol-% in He, Air Liquide) were co-saturated in the solution for at least 10 min. The very same electrodes, potentiostat and the electrochemical characterization procedure were used as described for the *in situ* measurements. The microelectrode was polished before each experiment.

Acknowledgements

Open Access funding enabled and organized by Projekt DEAL.

Conflict of Interest

The authors declare no conflict of interest.

Keywords: carbon dioxide reduction · cuprous oxide · scanning electrochemical microscopy · Raman microscopy · in situ characterization

[1] a) B. Zhang, J. Zhang, *J. Energy Chem.* **2017**, *26*, 1050; b) J. W. Vickers, D. Alfonso, D. R. Kauffman, *Energy Technol.* **2017**, *5*, 775.
[2] Y. Gao, Q. Wu, X. Liang, Z. Wang, Z. Zheng, P. Wang, Y. Liu, Y. Dai, M.-H. Whangbo, B. Huang, *Adv. Sci.* **2020**, *7*, 1902820.
[3] W. Fu, Z. Liu, T. Wang, J. Liang, S. Duan, L. Xie, J. Han, Q. Li, *ACS Sustainable Chem. Eng.* **2020**, *8*, 15223..
[4] Y. Wang, T. Jiang, D. Meng, J. Yang, Y. Li, Q. Ma, J. Han, *Appl. Surf. Sci.* **2014**, *317*, 414.
[5] C. M. McShane, K.-S. Choi, *J. Am. Chem. Soc.* **2009**, *131*, 2561.
[6] K. S. Adarsh, N. Chandrasekaran, V. Chakrapani, *Front. Chem.* **2020**, *8*, 137.
[7] W. Shan, R. Liu, H. Zhao, Z. He, Y. Lai, S. Li, G. He, J. Liu, *ACS Nano* **2020**, *14*, 11363..
[8] R. M. Arán-Ais, R. Rizo, P. Grosse, G. Algara-Siller, K. Dembélé, M. Plodinec, T. Lunkenbein, S. W. Chee, B. R. Cuenya, *Nat. Commun.* **2020**, *11*, 3489.
[9] a) D. Polcari, P. Dauphin-Ducharme, J. Mauzeroll, *Chem. Rev.* **2016**, *116*, 13234; b) J. Izquierdo, P. Knittel, C. Kranz, *Anal. Bioanal. Chem.* **2018**, *410*, 307.
[10] M. Michalak, A. Roguska, W. Nogala, M. Opallo, *Nanoscale Adv.* **2019**, *1*, 2645.
[11] T. Kai, M. Zhou, Z. Duan, G. A. Henkelman, A. J. Bard, *J. Am. Chem. Soc.* **2017**, *139*, 18552.
[12] Y. Kim, A. Jo, Y. Ha, Y. Lee, D. Lee, Y. Lee, C. Lee, *Electroanalysis* **2018**, *30*, 2861.
[13] a) N. Sreekanth, K. L. Phani, *Chem. Commun.* **2014**, *50*, 11143; b) N. Sreekanth, M. A. Nazrulla, T. V. Vineesh, K. Sailaja, K. L. Phani, *Chem. Commun.* **2015**, *51*, 16061.
[14] D. Filotás, T. Nagy, L. Nagy, P. Mizsey, G. Nagy, *Electroanalysis* **2018**, *30*, 690.
[15] M. Steimecke, G. Seiffarth, M. Bron, *Anal. Chem.* **2017**, *89*, 10679.
[16] a) M. Etienne, M. Dossot, J. Grausem, G. Herzog, *Anal. Chem.* **2014**, *86*, 11203; b) Z. T. Gossage, N. B. Schorr, K. Hernández-Burgos, J. Hui, B. H. Simpson, E. C. Montoto, J. Rodríguez-López, *Langmuir* **2017**, *33*, 9455.
[17] S. S. Hafner, S. Nagel, *Phys. Chem. Miner.* **1983**, *9*, 19.
[18] O. J. Rutt, G. R. Williams, S. J. Clarke, *Chem. Commun.* **2006**, 2869.
[19] T. Sander, C. T. Reindl, M. Giar, B. Eifert, M. Heinemann, C. Heiliger, P. J. Klar, *Phys. Rev. B* **2014**, *90*.
[20] F. A. Uribe, T. E. Springer, S. Gottesfeld, *J. Electrochem. Soc.* **1992**, *139*, 765.
[21] Q. Zhang, P. Liu, Z. Zhu, J. Zhang, F. Cao, *Corros. Sci.* **2020**, *164*, 108312.
[22] F. King, C. D. Litke, Y. Tang, *J. Electroanal. Chem.* **1995**, *384*, 105.
[23] J. Stotter, Y. Show, S. Wang, G. Swain, *Chem. Mater.* **2005**, *17*, 4880.
[24] M. Senthilkumar, J. Mathiyarasu, J. Joseph, K. L. N. Phani, V. Yegnaraman, *Mater. Chem. Phys.* **2008**, *108*, 403.
[25] D. Raciti, M. Mao, J. H. Park, C. Wang, *J. Electrochem. Soc.* **2018**, *165*, F799.

Manuscript received: September 10, 2021
Revised manuscript received: October 18, 2021
Accepted manuscript online: October 21, 2021